HOKKAIDO UNIVERSITY

Title	ON THE ISOTHERM FOR IONIC ADSORPTION FROM SOLUTION
Author(s)	BOCKRIS, J. O'M.; HABIB, M. A.
Citation	JOURNAL OF THE RESEARCH INSTITUTE FOR CATALYSIS HOKKAIDO UNIVERSITY, 23(1), 47-78
Issue Date	1976-01
Doc URL	https://hdl.handle.net/2115/24989
Type	departmental bulletin paper
File Information	23(1)_P47-78.pdf

Hokkaido University Collection of Scholarly and Academic Papers : HUSCAP

J. Res. Inst. Catalysis, Hokkaido Univ., Vol. 23, No. 1, pp. 47 to 78 (1975)

ON THE ISOTHERM FOR IONIC ADSORPTION FROM SOLUTION

By

J. O'M. BOCKRIS*) and M. A. HABIB*)

(Received March 24, 1975)

Abstract

The method of the Fourier-Bessel integral has been used to calculate the electrostatic image energy in the solution and to examine the effect on this quantity of diffuseness of the dielectric barrier in the double layer. The present diffuse dielectric boundary model shows an imaging energy in solution some 40 times less than that for a sharp boundary. The multiple energy is only 1% more than that of the single imaging in the metal.

An isotherm is deduced. The model used is the imaging in the metal; coulombic and dispersive interaction energies for the adsorbed ions are calculated without approximation; Flory-Huggins statistics are used. The capacitance charge curve is interpreted quantitatively with respect to the phenomenology of the capacitance hump and minimum. The hump is not significantly affected by the variation of the integral capacity with potential. The failure of the water model for capacitance hump is rationalized. The multiple imaging approximation using a sharp dielectric boundary does not predict a capacitance minimum (anodic) but predicts a capacitance hump which is in discrepance with experiment in respect to the ionic dependence and temperature.

Introduction

The deduction of adsorption isotherms for ionic substances on metals has been treated with two different approximations. In one[1,2], an isotherm emphasizing lateral repulsion between the ions on the surface, and with the approximation of the single imaging of the ion in the metal (imaging in the solution neglected) has been compared with experiment. The basis of this isotherm is the hitherto suppositional position that image energy *in solution*, calculated with a *non-sharp dielectric boundary*, between the inner Helmholtz plane and the rest of the solution will be negligible. In another approximation[5], the isotherm is based on multi-imaging in the metal and

*) School of Physical Sciences, the Flinders University of South Australia, Bedford Park, South Australia 5042

the solution. However, most of the publications on this model involve the approximation that the dielectric boundary between the inner layer and the solution is sharp, and therefore it has hitherto overestimated the energy of imaging in solution.

Numerical comparison of these models with experiment has been done too little. However, when done[2], it seems to favour the diffuse dielectric boundary (lateral repulsion) model. But the degree of discrepancy with experiment shown by the sharp dielectric boundary model is rendered negatory by the use of a constant value (for all ions) of a parameter, p, which represents the ratio of the area covered by an anion to that by a water molecule.

Among experimental data which bear upon the ability of the expressions based on either model to replicate experiment is the capacitance hump, where the lateral repulsion (diffuse dielectric boundary) approximation obtains good agreement between calculated and observed charges[2]. On this point, the sharp dielectric boundary model has not been tested, because, in it, the capacitance hump has been interpreted as due to water rotation[42].

Two new pieces of evidence have recently arisen to affect models for the double layer. According to SCHIFFRIN[8], the fluoride ion does undergo specific adsorption, and this removes an anomaly of the anion repulsion model for the capacitance hump, which has been developed from the diffuse dielectric boundary model[1]. Secondly, the experimental work of HILLS and PAYNE[10,11], and of HARRISON, RANDLES and SCHIFFRIN[9], together with the theoretical work of REEVES[7], and of BOCKRIS and HABIB[12], indicate that the maximum disorder of water molecules on the electrode surface comes on the negative side of the p. z. c. so that *the anodic hump* (which is always at anodic potentials) *cannot be explained in terms of water orientation.*

In the present paper, a smooth dielectric profile has been constructed on the basis of saturation of the dielectric near the electrode. The multiple imaging energy across this smoothly varying dielectric medium has been calculated and compared with the single image energy in the metal. The diffuse dielectric boundary (lateral repulsion) model is given in a second approximation which increases the applicability of the equation at higher θ's. Flory-Huggins statistics[13] have been introduced. Dispersive attraction between the ions[14] is taken into account and a quantitative interpretation of the capacitance minimum is given. A numerical comparison is made with an isotherm based on multiple imaging with respect to the properties of the hump, and other experimental observables.

1. The Dielectric Profile Across the Double Layer

The diffuse layer field is considered to affect the dielectric medium beyond the OHP. The dielectric constant is assumed to rise linearly from the first water layer to the OHP. The saturated value of six for the dielectric constant is assumed in the region of the first water layer.[1] The dielectric constant of the first layer consists of electronic and nuclear distortion polarization of the water molecule. Near to the potential of zero charge (p. z. c.), this is no longer true and the change of potential due to the changing orientation of dipoles, brought about by change of electrode charge, the basis to non-saturated orientation polarization of the water molecule layer adsorbed on the electrode, is allowed for in a separate equation.

The charge density in the diffuse layer is given by[15]

$$q_d = -2nze \sinh\frac{ze\phi}{kT} \tag{1.1}$$

where n, z, e, ϕ, are the number of ions per c.c., valency of ion, electronic charge and diffuse layer potential respectively (for a z-z electrolyte in solution).

The diffuse layer field, which takes into account the dielectric constant as a function of the field, can be represented by[41]:

$$\frac{d}{dx}(\varepsilon(\phi')\phi') = -4\pi q_d \tag{1.2}$$

where $\phi' = d\phi/dx$.
From (1.1) and (1.2),

$$\left[\phi'\varepsilon(\phi') + \phi'^2\frac{d\varepsilon(\phi')}{d\phi'}\right]d\phi' = +\left(8\pi nze \sinh\frac{ze\phi}{kT}\right)d\phi \tag{1.3}$$

Integration of both sides gives,

$$\phi'^2\varepsilon(\phi') - \int_0^{\phi'}\phi'\varepsilon(\phi')\,d\phi' = 8\pi nkT\left(\cosh\frac{ze\phi}{kT} - 1\right) \tag{1.4}$$

We apply BOOTH's theory[16] for variation of dielectric constant by applied field. GRAHAME[17] and LAIDLER[18] have shown that the variation of dielectric constant with field predicted by BOOTH's theory[16] is represented by the expression

$$\varepsilon(\phi') = \varepsilon_{\phi'\to\infty} + \frac{\varepsilon_0 - \varepsilon_\infty}{1 + b\phi'^2} \tag{1.5}$$

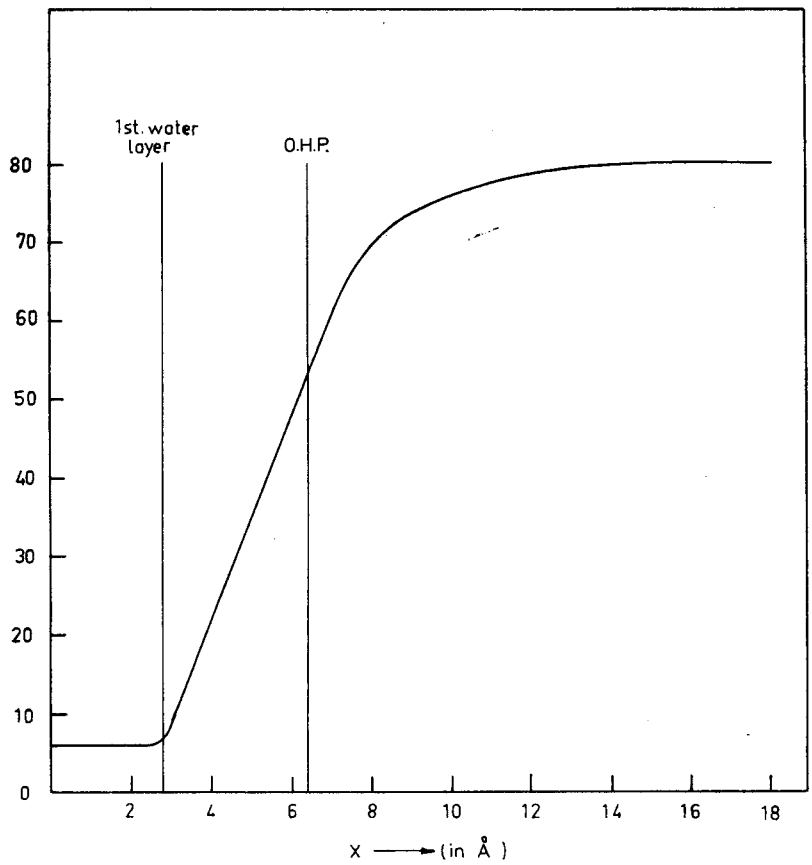

Fig. 1.1. The variation of dielectric constant with distance from the electrode surface.

where ε_0 is the dielectric constant at zero field strength, $b=1.08\times10^{-8}$ e.s.u., is a parameter found by GRAHAME to fit BOOTH's theory to experiment and $\varepsilon_{\phi'\to\infty}=\varepsilon_\infty$ is the fully saturated value of the dielectric constant of water.

Substitution of (1.5) in (1.4) and simplification gives rise to the dependence of ϕ upon ϕ', i.e.,

$$\phi=\frac{kT}{ze}\cosh^{-1}\xi \tag{1.6}$$

where

$$\xi=1+\frac{1}{8\pi nkT}\left[\frac{\varepsilon_\infty\phi'^2}{2}+\frac{(\varepsilon_0-\varepsilon_\infty)\phi'^2}{1+b\phi'^2}-(\varepsilon_0-\varepsilon_\infty)\frac{1}{2b}\ln(1+b\phi'^2)\right] \tag{1.7}$$

Now, the distance from the electrode surface, over which the potential varies, may be written as

$$x=\int \frac{dx}{d\phi}\,d\phi=\int \frac{1}{\phi'}\,\frac{d\phi}{d\phi'}\,d\phi' \tag{1.8}$$

Differentiating (1.6) w. r. t. ϕ', one gets,

$$\frac{d\phi}{d\phi'}=\frac{kT}{ze(\xi^2-1)^{1/2}}\left[\frac{\phi'}{8\pi nkT}\left\{\varepsilon_\infty+\frac{(\varepsilon_0-\varepsilon_\infty)}{1+b\phi'^2}\left(\frac{1-b\phi'^2}{1+b\phi'^2}\right)\right\}\right] \tag{1.9}$$

Substitution of (1.9) in (1.8) gives $x=f(\phi')$. $\varepsilon=f(\phi')$ is obtained from (1.5). Thus, from (1.5), (1.8) and (1.9), the variation of ε with distance x has been calculated numerically for a 0.1 N solution and is plotted in Fig. 1.1.

2. Multiple Image Interaction Energy with a Smoothly Varying Dielectric Constant

The dielectric constant-distance relation constructed in the last section may be considered to be a combination of a large number of dielectric slabs, schematically shown in Fig. 2.1. The interaction energy, which corresponds to the energy of a single charge in multiple imaging across a number of dielectric plates can be obtained by the method of the Fourier-Bessel integral.[19~21] Since a smooth dielectric profile can be regarded as a combination of an infinite number of infinitesimally thin dielectric media, we first find the interaction energy across the first few dielectric slabs, respectively and, by analogy to the first four expressions, find out the expression representing the interaction energy across an infinite number of such slabs.

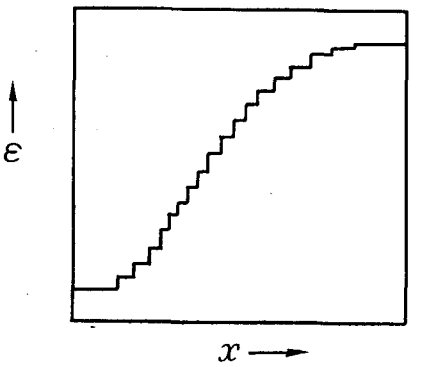

Fig. 2.1. Schematic representation of dielectric constant of a solution phase as a combination of a large number of dielectric slabs.

2.1 *Energy across two dielectric slabs*

This corresponds to a situation where there is a sharp dielectric discontinuity on the solution side. The interaction energy of a charge situated in the IHP with its images in the metal and solution (Fig. 2.1.1) is given by (cf. SMYTHE)[19]

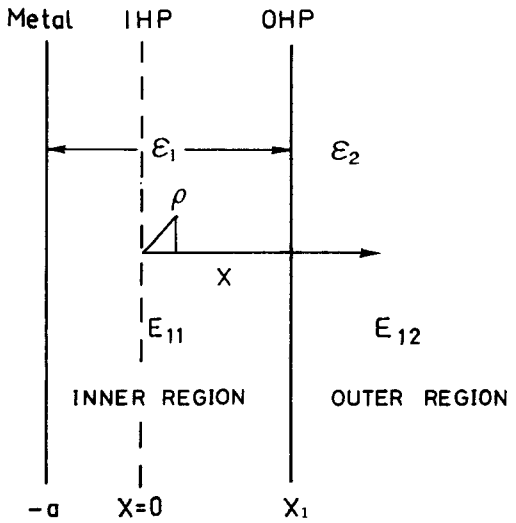

Fig. 2.1.1. Relative positions of the planes of dielectric discontinuity at the metal ($x=-a$) and at the OHP ($x=x_1$).

$$E_{11}=\frac{e^2}{\varepsilon_1}\left\{\int_0^\infty J_0(k\rho)\,e^{-k|x|}\,dk+\int_0^\infty a_{11}(k)\,J_0(k\rho)\,e^{kx}dk+\int_0^\infty b_{11}(k)\,J(k\rho)\,e^{-kx}dk\right\} \tag{2.1.1}$$

where $J_0(k\rho)$ is the Bessel function of the first kind of zero order. In region 2,

$$E_{12}=\frac{e^2}{\varepsilon_1}\int_0^\infty a_{2-\infty}(k)\,J_0(k\rho)\,e^{-kx}dk \tag{2.1.2}$$

Using the boundary conditions, the potential (E_{11}/e) is zero at $x=-a$ and continuous at $x=x_1$; and $\varepsilon_1\,\partial(E_{11}/e)/\partial x|_{x=x_1}=\varepsilon_2\,\partial(E_{12}/e)/\partial x|_{x=x_1}$, the functions $a_{11}(k)$ and $b_{11}(k)$ are evaluated to be:

$$a_{11}(k)=-\frac{\beta_1 e^{-2kx_1}(1-e^{-2ka})}{1-\beta_1 e^{-2k(x_1+a)}} \tag{2.1.3}$$

and

$$b_{11}(k)=\frac{-e^{-2ka}+\beta_1 e^{-2k(x_1+a)}}{1-\beta_1 e^{-2k(x_1+a)}} \tag{2.1.4}$$

where $\beta_1=(\varepsilon_2-\varepsilon_1)/(\varepsilon_2+\varepsilon_1)$.

Substituting (2.1.3) and (2.1.4) in (2.1.1), neglecting the self interaction term, and evaluating at $x=0$ and $\rho=0$, one gets:

$$E_{11}=\frac{e^2}{\varepsilon_1}\left[\int_0^\infty -e^{-2k\alpha}dk-\int_0^\infty \frac{\beta_1 e^{-2kx_1}(1-e^{-2k\alpha})^2}{1-\beta_1 e^{-2k(x_1+\alpha)}}dk\right] \qquad (2.1.5)$$

Eqn. (2.1.5) represents the total energy of a charge at $x=0$, $\rho=0$ (see Fig. 2.1.1.), and it takes into account the imaging energy of the ion in the position shown in Fig. 2.1.1, both with respect to its energy in the metal and also that in the solution: and the energy resulting from multiple electrostatic reflections in the solution and in the metal.

2.2 *Energy across three dielectric slabs*

If the solution side is considered to be a combination of three dielectric media, one with the dielectric constant ε_1 in which the charge is situated (region 1) and other two with dielectric constants ε_2 and ε_3 (Fig. 2.2.1), then the energies in the three regions are given by:

$$E_{12}=\frac{e^2}{\varepsilon_1}\left\{\int_0^\infty J_0(k\rho)\,e^{-k|x|}dk+\int_0^\infty a_{21}(k)\,J_0(k\rho)\,e^{+kx}dk+\int_0^\infty b_{21}(k)\,J_0(k\rho)\,e^{-kx}dk\right\} \qquad (2.2.1)$$

where E_{12} means the interaction of a charge in 1 with images in the metal and with the images in the dielectric medium 2.

$$E_{22}=\frac{e^2}{\varepsilon_1}\left\{\int_0^\infty a_{22}(k)\,J_0(k\rho)\,e^{-kx}dk+\int_0^\infty b_{22}(k)\,J_0(k\rho)\,e^{kx}dk\right\} \qquad (2.2.2)$$

where E_{22} signifies the interaction of a charge in region 2 with its image in the metal and with the image in the dielectric in regions 1 and 3.

Similarly,

$$E_{32}=\frac{e^2}{\varepsilon_1}\int_0^\infty a_{23}(k)\,J_0(k\rho)\,e^{-kx}dk \qquad (2.2.3)$$

where this energy is the energy of a charge situated in 3 with the image

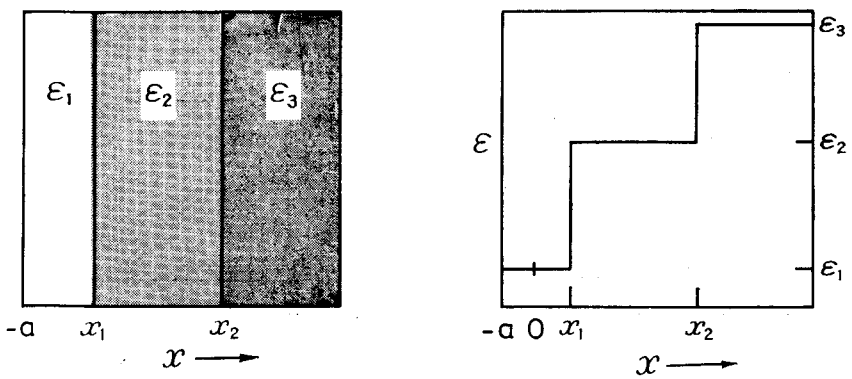

Fig. 2.2.1. Electrolyte solution as a combination of three dielectric phases.

in metal and those in 1 and 2.

Using the respective boundary conditions, the functions $a_{21}(k)$ and $b_{21}(k)$ are found to be

$$a_{21}(k)=\frac{(1-e^{-2ka})\,e^{-2kx_1}}{e^{-2k(x_1+a)}-\dfrac{1+\beta_1\beta_2 e^{-2kd_1}}{\beta_1+\beta_2 e^{-2kd_1}}} \tag{2. 2. 4}$$

and

$$b_{21}=-e^{-2ka}-\frac{e^{-2k(x_1+a)}(1-e^{-2ka})}{e^{-2k(x_1+a)}-\dfrac{1+\beta_1\beta_2 e^{-2kd_1}}{\beta_1+\beta_2 e^{-2kd_1}}} \tag{2. 2. 5}$$

where $d_1=x_2-x_1$, and $\beta_2=(\varepsilon_3-\varepsilon_2)/(\varepsilon_3+\varepsilon_2)$.

With (2. 2. 1), (2. 2. 4) and (2. 2. 5), one finds

$$E_{12}=\frac{e^2}{\varepsilon_1}\left\{\int_0^\infty -e^{-2ka}dk-\int_0^\infty \frac{e^{-2kx_1}(1-e^{-2ka})^2}{\dfrac{1+\beta_1\beta_2 e^{-2kd_1}}{\beta_1+\beta_2 e^{-2kd_1}}-e^{-2k(x_1+a)}}dk\right\} \tag{2. 2. 6}$$

2. 3 *Energy across four dielectric plates*

In this case, the multiple image energies in the different regions (Fig. 2. 3. 1) are

$$E_{13}=\frac{e^2}{\varepsilon_1}\left\{\int_0^\infty J_0(k\rho)\,e^{-k|z|}dk+\int_0^\infty a_{31}(k)\,J_0(k\rho)\,e^{+kz}dk+\int_0^\infty b_{32}(k)\,J_0(k\rho)\,e^{-kz}dk\right\} \tag{2. 3. 1}$$

$$E_{23}=\frac{e^2}{\varepsilon_1}\left\{\int_0^\infty a_{32}(k)\,J_0(k\rho)\,e^{-kz}dk+\int_0^\infty b_{32}(k)\,J_0(k\rho)\,e^{+kz}dk\right\} \tag{2. 3. 2}$$

$$E_{33}=\frac{e^2}{\varepsilon_1}\left\{\int_0^\infty a_{33}(k)\,J_0(k\rho)\,e^{-kz}dk+\int_0^\infty b_{33}(k)\,J_0(k\rho)\,e^{+kz}dk\right\} \tag{2. 3. 3}$$

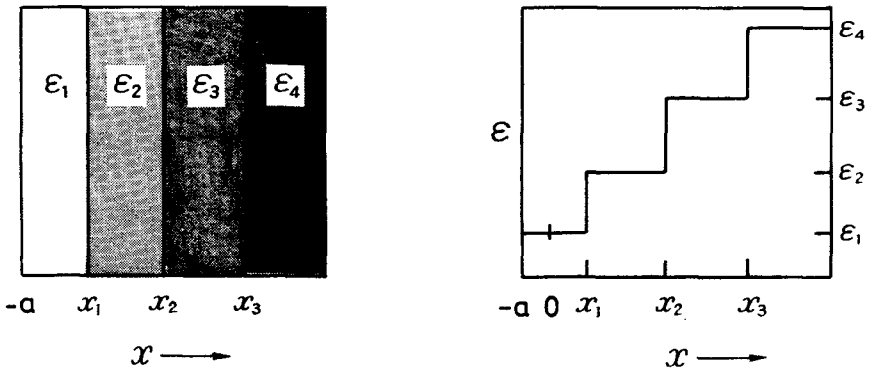

Fig. 2. 3. 1. Combination of four dielectric media representing the solution phase.

and

$$E_{43}=\frac{e^2}{\varepsilon_1}\left\{\int_0^\infty a_{34}(k)\,J_0(k\rho)\,\mathrm{e}^{-kx}\mathrm{d}k\right\} \tag{2. 3. 4}$$

The functions $a_{31}(k)$ and $b_{31}(k)$ are found to be

$$a_{31}(k)=-\frac{(1-\mathrm{e}^{-2k\alpha})\,\mathrm{e}^{-2kx_1}}{\dfrac{1+\beta_1\beta_2\mathrm{e}^{-2kd}+\beta_2\beta_3\mathrm{e}^{-2kd}+\beta_1\beta_3\mathrm{e}^{-4kd}}{\beta_1+(\beta_2+\beta_1\beta_2\beta_3)\,\mathrm{e}^{-2kd}+\beta_3\mathrm{e}^{-4kd}}-\mathrm{e}^{-2k(x_1+\alpha)}} \tag{2. 3. 5}$$

where $d_2=x_3-x_2=d_1=x_2-x_1=d$
and

$$b_{31}(k)=-\mathrm{e}^{-2k\alpha}+\frac{\mathrm{e}^{-2k(x_1+\alpha)}\,(1-\mathrm{e}^{-2k\alpha})}{\dfrac{1+(\beta_1\beta_2+\beta_2\beta_3)\,\mathrm{e}^{-2kd}+\beta_1\beta_3\mathrm{e}^{-4kd}}{\beta_1+(\beta_2+\beta_1\beta_2\beta_3)\,\mathrm{e}^{-2kd}+\beta_3\mathrm{e}^{-4kd}}-\mathrm{e}^{-2k(x_1+\alpha)}} \tag{2. 3. 6}$$

With (2. 3. 1), (2. 3. 5) and (2. 3. 6), one finds

$$E_{13}=\frac{e^2}{\varepsilon_1}\left\{\int_0^\infty -\mathrm{e}^{-2k\alpha}\mathrm{d}k-\int_0^\infty \frac{\mathrm{e}^{-2kx_1}\,(1-\mathrm{e}^{-2k\alpha})^2}{\dfrac{1+(\beta_1\beta_2+\beta_2\beta_3)\,\mathrm{e}^{-2kd}+\beta_1\beta_3\mathrm{e}^{-4kd}}{\beta_1+(\beta_2+\beta_1\beta_2\beta_3)\,\mathrm{e}^{-2kd}+\beta_3\mathrm{e}^{-4kd}}-\mathrm{e}^{-2k(x_1+\alpha)}}\mathrm{d}k\right\} \tag{2. 3. 7}$$

2. 4 *Energy across five dielectric plates*

When the region having varying dielectric constant is considered to be a combination of five dielectric media (Fig. 2. 4. 1), following the procedure described above, the image interaction energy of a charge situated in region 1, is given by,

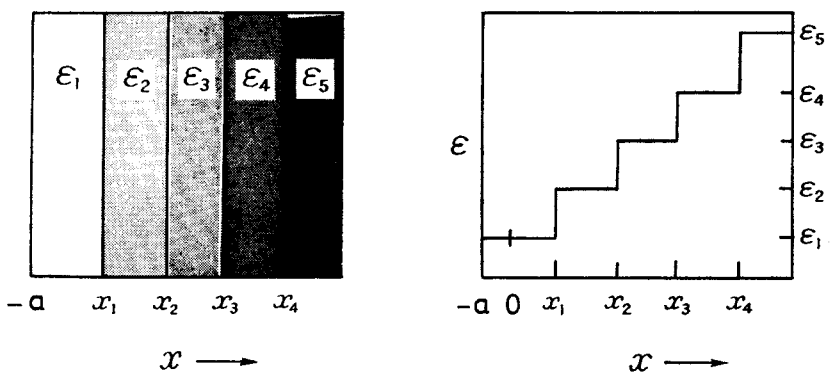

Fig. 2. 4. 1. Representation of solution phase by five dielectric slabs.

$$E_{14}=\frac{e^2}{\varepsilon_1}\left[\int_0^\infty -e^{-2ka}dk-\int_0^\infty \frac{e^{-2kx_1}(1-e^{-2ka})^2}{1+(\beta_1\beta_2+\beta_2\beta_3+\beta_3\beta_4)e^{-2kd}+(\beta_1\beta_3+\beta_2\beta_4+\beta_1\beta_2\beta_3\beta_4)e^{-4kd}+\beta_1\beta_4e^{-6kd}}{\beta_1+(\beta_2+\beta_1\beta_2\beta_3+\beta_1\beta_3\beta_4)e^{-2kd}+(\beta_3+\beta_1\beta_2\beta_4+\beta_2\beta_3\beta_4)e^{-4kd}+\beta_4e^{-6kd}}-e^{-2k(x_1+a)}dk\right] \tag{2.4.1}$$

2.5 *Energy across smoothly varying dielectric medium*

In reality, the dielectric constant increases from its saturated lower value to its highest bulk value over a certain distance, depending on the strength of the saturating field. This smoothly varying dielectric profile may be assumed to be a combination of an infinite number of infinitesimally thin dielectric media (i. e., $d\to 0$). By analogy to equations (2. 1. 5), (2. 2. 6), (2. 3. 7) and (2. 4. 1), the total multiple image interaction energy of a charge situated on IHP across the real varying dielectric medium may be represented by

$$E_T=\frac{e^2}{\varepsilon_1}\left\{\int_0^\infty -e^{-2ka}dk-\int_0^\infty \frac{e^{-2kx_1}(1-e^{-2ka})^2\sum_{n=0}^{\infty}\beta_{n+1}e^{-2nkd}}{1+\beta_1\sum_{n=1}^{\infty}\beta_{n+1}e^{-2nkd}-e^{-2k(x_1+a)}\sum_{n=0}^{\infty}\beta_{n+1}e^{-2nkd}}dk\right\} \tag{2.5.1}$$

where $\beta_n=(\varepsilon_{n+1}-\varepsilon_n)/(\varepsilon_{n+1}+\varepsilon_n)$, where n is an integer. (2. 5. 2)

The above integral is to be solved for a condition when $d\to 0$ (hence $\beta_n\to 0$). To solve this, one needs an analytical expression for β_n as a function of x (distance) i. e., $\varepsilon=f(x)$. To serve our purpose, we represent the dielectric curve (Fig. 1.1) by the empirical expression :

$$\varepsilon(x)=a_1+a_2x+a_3x^2+a_4x^3+a_5x^4 \tag{2.5.3}$$

where a_1, a_2, a_3, a_4 and a_5 are constants.

β_n can now be represented by

$$\beta_n=\frac{\varepsilon_{(x_n+\Delta x)}-\varepsilon_{(x_n)}}{\varepsilon_{(x_n+\Delta x)}+\varepsilon_{(x_n)}}\approx\frac{\Delta\varepsilon(x)}{2\varepsilon_n(x)} \tag{2.5.3a}$$

where,

$$\varepsilon_{(x_n)}=a_1+a_2x_n+a_3x_n^2+a_4x_n^3+a_5x_n^4 \tag{2.5.4}$$

and

$$\varepsilon_{(x_n+\Delta x)}=a_1+a_2(x_n+\Delta x)+a_3(x_n+\Delta x)^2+a_4(x_n+\Delta x)^3+a_5(x_n+\Delta x)^4 \tag{2.5.5}$$

Since $d=\Delta x\to 0$, one gets, neglecting higher power terms in d,

$$\beta_n=\frac{\mathrm{d}(a_2+2a_3x_n+3a_4x_n^2+4a_5x_n^3)}{2\varepsilon_n}=R_nd \tag{2.5.6}$$

where $$R_n=\frac{a_2+2a_3x_n+3a_4x_n^2+4a_5x_n^3}{2\varepsilon_n} \tag{2.5.7}$$

Substituting (2.5.6) in (2.5.1) and neglecting $0(d^2)$ terms, (2.5.1) reduces to

$$\begin{aligned}E_{\mathrm{T}}&=\frac{e^2}{\varepsilon_1}\left\{\int_0^\infty -\mathrm{e}^{-2ka}\mathrm{d}k-\int_0^\infty \mathrm{e}^{-2kx_1}(1-\mathrm{e}^{-2ka})^2\,d\sum_{n=0}^{\infty}R_{n+1}\mathrm{e}^{-2knd}\mathrm{d}k\right\}\\&=\frac{e^2}{\varepsilon_1}\left[-\frac{1}{2a}-d\sum_{n=0}^{\infty}R_{n+1}\left\{\frac{1}{2(x_1+nd)}-\frac{2}{2(x_1+a+nd)}\right.\right.\\&\left.\left.+\frac{1}{2(x_1+2a+nd)}\right\}\right]\end{aligned} \tag{2.5.8}$$

Since $d\to 0$, the summation can be replaced by an integral and E_{T} is represented by

$$E_{\mathrm{T}}=\frac{e^2}{\varepsilon_1}\left[-\frac{1}{2a}-\frac{1}{2}\int_{b_1}^{b_2}R(x)\left\{\frac{1}{x_1+x}-\frac{2}{x_1+a+x}+\frac{1}{x_1+2a+x}\right\}\mathrm{d}x\right] \tag{2.5.9}$$

where b_2-b_1 is the length over which dielectric constant varies and $R(x)$ is given by (2.5.7). The constants in (2.5.4) were determined by simultaneous solution of a set of linear equations representing Fig. (1.1) and the integral in (2.5.9) was solved numerically by SIMPSON's rule on an IBM-1130 computer. With $a=2$Å, and $x_1=2$Å, we get:

$$E_{\mathrm{T}}=-\frac{e^2}{\varepsilon_1}\ (0.253102\times 10^8\ \mathrm{cm}^{-1}) \tag{2.5.10}$$

The interaction energy of an adsorbed charge on the IHP with its single image in the metal is:

$$E_{\mathrm{S}}=-\frac{e^2}{2\varepsilon_1 a}=-\frac{e^2}{\varepsilon_1}\ (0.25\times 10^8\ \mathrm{cm}^{-1}) \tag{2.5.11}$$

Thus, the multiple image energy with a consideration of continuous variation of dielectric constant is $\{(E_{\mathrm{T}}-E_{\mathrm{S}})/E_{\mathrm{S}}\}\times 100\simeq 1\%$ more than the single image energy.

If the dielectric boundary at a distance $x_1=2$Å is assumed to be sharp, then the total energy (including the multiple imaging) which is represented by the eqn. 2.1.5, comes out to be $E_{11}=-(e^2/\varepsilon_1)\ (0.3450\times 10^8\ \mathrm{cm}^{-1})=1.38E_{\mathrm{S}}$.

If the dielectric boundary were sharp, therefore, it *would* be important to use *multiple* imaging but the situation in the solution is that there is no sharp dielectric boundary, and hence a model based on such a model will be a less good approximation than one based on a more realistic, diffuse, boundary. The correctness of this assertion will be tested below by a comparison of the abilities of discrete and diffuse approaches to replicate experiment.

These conclusions have been reached on the basis of considering a single ion and its imaging along one x coordinate. The calculation of the interaction energy on the electrode surface involves interaction along a y coordinate. Here, too, the only imaging energy of numerical significance is that of the ion imaging across the *sharp solution-metal* boundary. This conclusion takes into account the fact that the repulsion energy between the ions in the surface is reduced by imaging. The value of 1% extra energy due to multiple imaging obtained above is in comparison with the *single* image energy of an ion in the electrode. In the complete sum of the interaction of a reference ion with all the images (in solution and in the metal), the reference situation should be the sum of all interactions of a central ion with the other ions on the surface and their single images, together with the same situation using the multiple image picture. There is no reason to think that a significantly greater ratio would come out of this more complex situation by multiple imaging than that of the simpler and more basic case worked out above.*)

Therefore, in the next section, while calculating the image interaction energy, we consider the interaction of a reference ion with single images of other adsorbed ions, but we shall neglect the result of their images in solution across the continuously varying dielectric medium. It is our submission that this offers a better approximation than that of accounting for the solution imaging in such a diffuse boundary.

3. Evaluation of the Lateral Interaction Energy

Consider a reference ion, surrounded by a hexagonal array of ions, effectively in concentric rings of radii $1r$, $2r$, $\cdots$ nr. There are $6n$ ions in the n-th ring. The interaction energy between the reference ion and ions on the n-th ring, and their images, is[22]:

*) An accurate calculation in three dimension with smoothly varying dielectric medium would be mathematically impractical so that this 1% energy has been neglected.

$$U_r = \frac{6e^2}{\varepsilon r}\left[1-\frac{1}{\left[1+\left(\frac{2r_i}{nr}\right)^2\right]^{1/2}}\right]^{*)}, \tag{3.1}$$

where r_i is the ionic radius.

Correspondingly,

$$r = \left(\frac{4}{n_A\pi}\right)^{1/2} = \left(\frac{4e}{\pi Q_{max}}\right)^{1/2} \tag{3.2}$$

where θ is the fractional of the surface covered with ions, n_A per unit area, which contact (or specifically) adsorbed; and Q_{max} is the maximum amount of contact-adsorbed charge, where:

$$Q_{max} = \frac{e}{4r_i^2} \tag{3.3}$$

Hence:

$$r = \frac{4r_i}{\pi^{1/2}\theta^{1/2}} \tag{3.4}$$

(3.4) into (3.1) gives for the total lateral coulombic interaction of all ions with the central ion:

$$E_{Lat} = \frac{3}{2}\frac{\pi^{1/2}e^2\theta^{1/2}}{\varepsilon r_i}\sum_{n=1}^{\infty}\left\{1-\left(1+\frac{\pi\theta}{4n^2}\right)^{-1/2}\right\} \tag{3.5}$$

4. Evaluation of Dispersion Energy

Now[23~25],

$$U_{disp.1} = -\frac{3}{4}\frac{h\nu}{\varepsilon_{opt}r^6}\alpha^2\sqrt{s}\ , \tag{4.1}$$

where ν is the frequency occurring in dispersive coupling between two like ions; α is their polarisability, and s is the number of electrons in the outer shell. In the dispersive interaction between the ions in the n-th ring and the central ion,

$$U_{disp.2} = -\frac{3}{4}\frac{h\nu\alpha^2 6n}{\varepsilon_{opt}(nr)^6}\sqrt{s} \tag{4.2}$$

The dispersion energy of one ion with the image ions of the n-th ring is:

---

*) In earlier work[1], this expression was expanded binomially to 3 terms, because $\pi\theta/4n^2<1$. We are grateful to Dr. S. LEVINE for showing us that, even though the binomial expansion to three terms is accurate to 1%, such an expansion is inadequate to represent the lateral interaction at high coverage.

$$U_{\text{disp},3} = -\frac{3}{4}\frac{h\nu\alpha^2}{\varepsilon_{\text{opt}}[\{(nr)^2+(2r_i)^2\}^{1/2}]^6}\cdot 6n\sqrt{s} \tag{4.3}$$

Taking $U_{\text{disp},2}+U_{\text{disp},3}$, and using r from (3.4), the total dispersion attraction of all ions with the central ion is:

$$U_{\text{disp}} = -\frac{18}{4^7}\frac{h\nu\alpha^2\pi^3\theta^3\sqrt{s}}{\varepsilon_{\text{opt}}r_i^6}\sum_{n=1}^{\infty}\frac{1}{n^5}\left[1+\frac{1}{\left[1+\frac{\pi\theta}{4n^2}\right]^3}\right] \tag{4.4}$$

5. Deduction of the Isotherm

The standard free energy of adsorption ΔG^0_{ads} depends, amongst other factors, on how many solvent molecules are displaced by the adsorption of an ion. The ionic adsorption from solution can be represented by the following quasi-chemical substitution process in the interphase:

$$\text{Ions (in soln)}+p\text{H}_2\text{O (ads)} \leftrightarrows \text{Ions (ads)}+p\text{H}_2\text{O (in soln)} \tag{5.1}$$

where p is number of water molecules displaced by an ion upon adsorption. At equilibrium,

$$\mu_{i,\text{ads}}-p\mu_{w,\text{ads}} = \mu_{i,\text{soln}}-p\mu_{w,\text{soln}} \tag{5.2}$$

where μ's refer to the chemical potential of the species denoted by subscripts.

Using Flory-Huggin's statistics, $\mu_{i,\text{ads}}$ and $\mu_{w,\text{ads}}$ are given by[26]

$$\mu_{i,\text{ads}} = -kT\ln q_2 + kT\ln\frac{\theta}{\exp[(p-1)(1-\theta)]} \tag{5.3}$$

and

$$\mu_{w,\text{ads}} = -kT\ln q_1 + kT\ln\left[\frac{(1-\theta)}{\exp\left(\frac{\theta}{p}-\theta\right)}\right] \tag{5.4}$$

where q_1 and q_2 are the internal partition functions of the water molecules and ions respectively and θ is the fraction of the surface covered by the ions. $\mu_{i,\text{soln}}$ and $\mu_{w,\text{soln}}$ are represented as

$$\mu_{i,\text{soln}} = \mu^0_{i,\text{soln}} + RT\ln X_{i,\text{soln}} \tag{5.5}$$

$$\mu_{w,\text{soln}} = \mu^0_{w,\text{soln}} + RT\ln X_{w,\text{soln}} \tag{5.6}$$

where $X_{i,\text{soln}}$ and $X_{w,\text{soln}}$ are the mole fractions of ions and water molecules in solution, respectively.

Substituting (5.3)~(5.6) in (5.2) one gets

$$\frac{\theta}{e^{p-1}(1-\theta)^p} = \frac{X_{i,soln}}{(X_{w,soln})^p} e^{-\Delta G^0/RT} \tag{5.7}$$

where $$\Delta G^0 = (-kT \ln q_2 - \mu^0_{i,soln}) - (pkT \ln q_1 - p\mu^0_{w,soln}). \tag{5.8}$$

Using the site fraction statistics to express the bulk phase concentrations, (5.7) can be written as,

$$\frac{\theta}{pe^{p-1}(1-\theta)^p} = N \exp\left(-\frac{\Delta G^0}{RT}\right) \tag{5.9}$$

where

$$N = \left[\frac{C_i(pC_i + C_w)^{p-1}}{C_w^p}\right] \tag{5.10}$$

where C's refer to concentrations.

We separate ΔG^0 into two terms,

(a) ΔG^0_c, which represents a coverage-independent term for the interaction of ion and electrode (i. e., metal-ion dispersion; partial dehydration, etc.).

and

(b) $\Delta G^0_i = U_{Lat} + U_{Disp} + U_{2-1}$

The work done to bring an ion from the Helmholtz layer to the electrode is given by:

$$U_{2-1} = -\frac{4\pi q_M(x_2 - x_1)}{\varepsilon_1} \tag{5.11}$$

where q_M is the electrode charge, x_2 and x_1 are the distances of the outer Helmholtz plane (OHP) and inner Helmholtz plane (IHP) respectively from the metal surface and ε_1 is the mean dielectric constant of the medium between the OHP and the IHP. In Fig. 1.1 the dielectric constant falls greatly from the OHP to the 1st water layer but thereafter remains constant at about 6. The major part of the work represented by equation (5.11) is done in this region and this is the background of the approximate use of a value of 6 in equation (5.11). Substituting for U_{Lat}, U_{Disp} and U_{2-1}, the ionic adsorption isotherm takes the form:

$$\frac{\theta}{pe^{p-1}(1-\theta)^p} = N \exp\left[-\frac{\Delta G^0_c}{RT} + \frac{4\pi q_M(x_2 - x_1)}{\varepsilon_1 kT} - \frac{3}{2}\frac{e^2\pi^{1/2}\theta^{1/2}}{\varepsilon_1 r_1 kT}\sum_{n=1}^{\infty}\left\{1 - \left[1 + \frac{\pi\theta}{4n^2}\right]^{-1/2}\right\} + \frac{18}{4^7}\frac{h\nu\alpha^2\pi^3\theta^3}{\varepsilon_{opt} kT r_i^6}\sqrt{s}\sum_{n=1}^{\infty}\frac{1}{n^5}\left\{1 + \frac{1}{\left[1 + \frac{\pi\theta}{4n^2}\right]^3}\right\}\right] \tag{5.12}$$

Eqn. (5.12) can be rearranged to give

$$\ln\frac{\theta}{p e^{p-1}(1-\theta)^p} = \ln N - \frac{\Delta G_c^0}{RT} + Aq_M - C\sqrt{\theta}\sum_{n=1}^{\infty}\left\{1-\frac{1}{\left(1+\frac{\pi\theta}{4n^2}\right)^{1/2}}\right\}$$

$$+ D\theta^3\sum_{n=1}^{\infty}\frac{1}{n^5}\left\{1+\frac{1}{\left(1+\frac{\pi\theta}{4n^2}\right)^3}\right\} \qquad (5.13)$$

where,

$$A = \frac{4\pi e(x_2-x_1)}{\varepsilon_1 kT}, \qquad C = \frac{3}{2}\frac{e^2\pi^{1/2}}{\varepsilon_1 r_1 kT},$$

and

$$D = \frac{18}{4^7}\frac{h\nu\alpha^2\pi^3}{\varepsilon_{opt}kTr_1^6}\sqrt{s} \qquad (5.14)$$

6. Prediction of Inflection Points on the θ-q_M Curve

Differentiating (5.13) w. r. t. q_M, one gets,

$$\frac{d\theta}{dq_M} = \frac{A}{\frac{1+\theta(p-1)}{\theta(1-\theta)} + \frac{C}{2\sqrt{\theta}}\sum_{n=1}^{\infty}\left\{1-\left(1+\frac{\pi\theta}{4n^2}\right)^{-3/2}\right\} - 3D\theta^2\sum_{n=1}^{\infty}\frac{1}{n^5}\left\{1+\left(1+\frac{\pi\theta}{4n^2}\right)^{-4}\right\}} \qquad (6.1)$$

An inflection on the θ-q_M plot will occur when

$$\frac{d^2\theta}{dq_M^2} = 0$$

i. e., when,

$$\frac{2\theta-1+\theta^2(p-1)}{\theta^2(1-\theta)^2} + \frac{C}{4\theta^{3/2}}\sum_{n=1}^{\infty}\left\{\frac{1+\frac{\pi\theta}{n^2}}{\left(1+\frac{\pi\theta}{4n^2}\right)^{5/2}}-1\right\} - 6D\theta\sum_{n=1}^{\infty}\frac{1}{n^5}\left[1+\frac{\left(1-\frac{\pi\theta}{4n^2}\right)}{\left(1+\frac{\pi\theta}{4n^2}\right)^5}\right] = 0 \qquad (6.2)$$

Calculation of D involves a choice of the parameters ν and α. The frequency ν can be calculated from:

$$\nu = \frac{e}{2\pi\sqrt{M\alpha}} = \frac{3.581\times10^3}{\sqrt{\alpha}} \qquad (6.3)$$

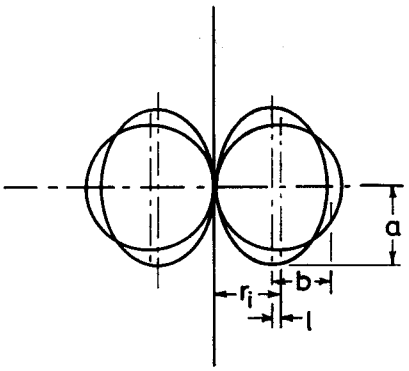

Fig. 6. 1. The displacement of ionic centre by the image field.

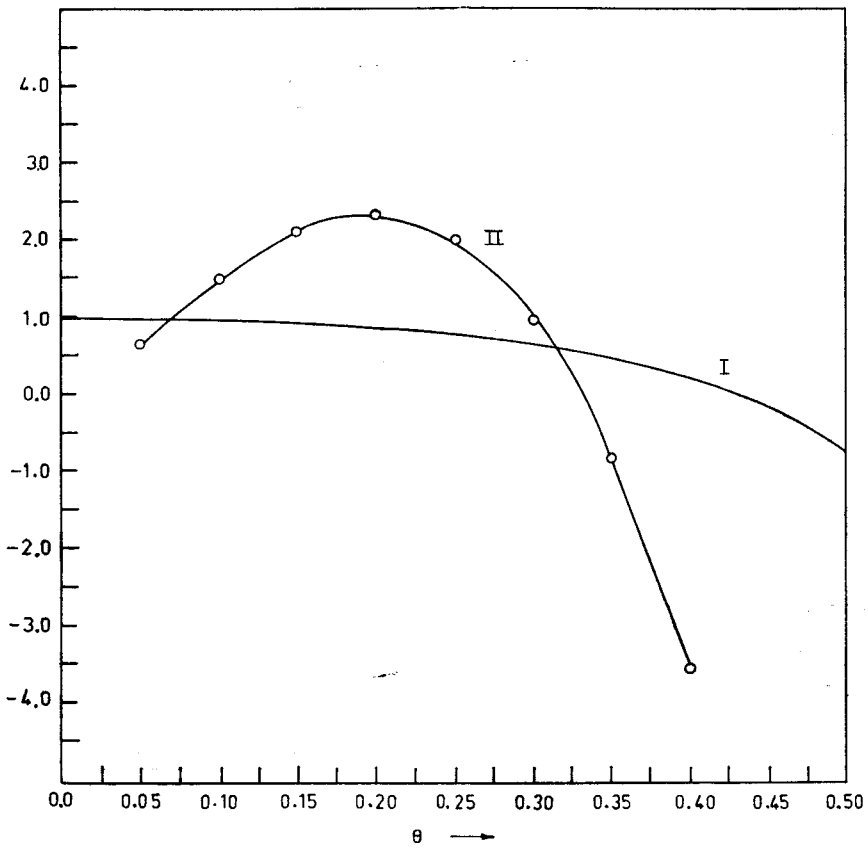

Fig. 6. 2 (a). The functions $Z_1(\theta)$(I) and $Z_2(\theta)$(II) against θ for Cl^-

TABLE 1. The values of the parameters used in eqn. (6.2)

	Ions	Raddi (Å)*)	$\nu \times 10^{-15}$/sec	S	P
Monoatomic Ions	Cl^-	1.81	1.167	8	1.72
	Br^-	1.96	1.035	8	2.00
	I^-	2.19	0.877	8	2.52
Polyatomic Ions	ClO_3^-	2.43	0.750	15	3.10
	BrO_3^-	2.43	0.750	15	3.10
	ClO_4^-	2.54	0.702	17	3.39
	NO_3^-	2.61	0.674	13	3.58
	SCN^-	1.60	1.404	9	1.34

*) The radii of halides are assumed as their crystallographic radii. The effective radii of ClO_3^-, BrO_3^-, ClO_4^- and SCN^- are taken from the reference 32, and that of NO_3^- is noted from ref. 33.

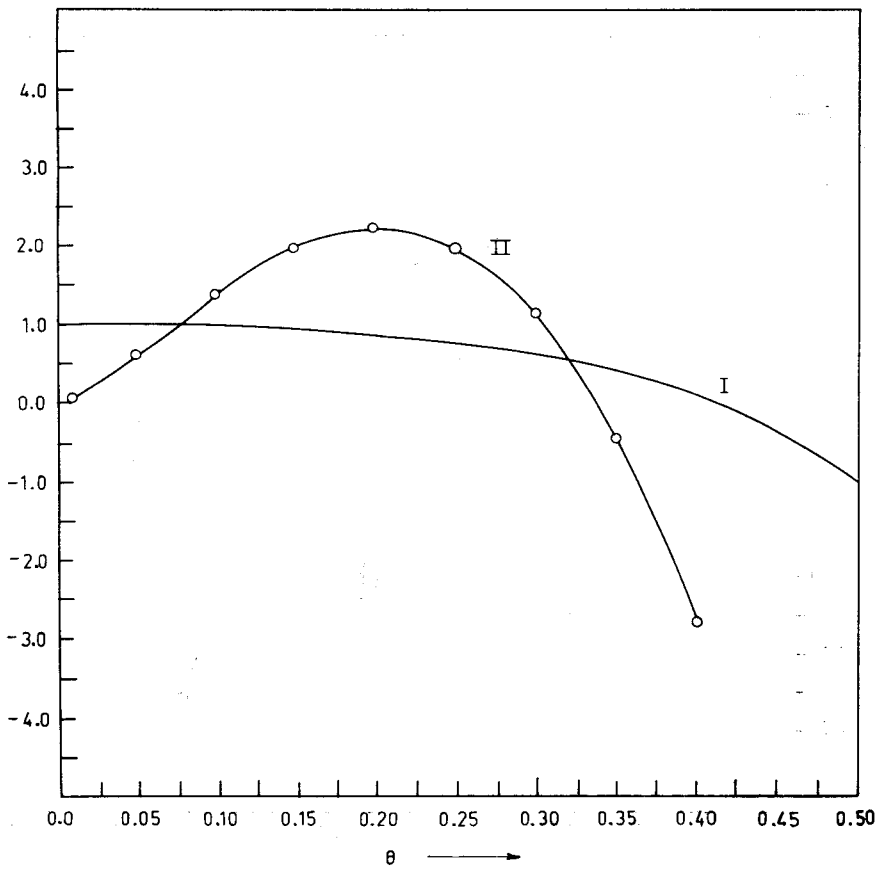

Fig. 6.2(b). The functions $Z_1(\theta)$(I) and $Z_2(\theta)$(II) against θ for Br^-

TABLE 2. The values of $-d^2y/d\theta^2$ and constituent terms in eqn. (7.6) corresponding to θ_1.

Ions	θ_1	1st term	2nd term	3rd term	$-d^2y/d\theta^2$
Cl^-	0.0700	−5835.1805	−1970.1657	242.0326	−3622.9822
Br^-	0.0750	−4745.7947	−1660.2041	211.0342	−2874.5565
I^-	0.0820	−3633.8563	−1302.2831	174.5468	−2157.0264
ClO_3^-	0.1000	−2008.5048	−879.0123	192.8964	−936.5961
BrO_3^-	0.1000	−2008.5048	−879.0123	192.8964	−936.5961
ClO_4^-	0.0950	−2341.8487	−868.5039	193.4390	−1279.9057
NO_3^-	0.1000	−2009.8217	−818.3908	161.3795	−1030.0512
SCN^-	0.0650	−7285.9369	−2505.0000	314.4858	−4466.4510

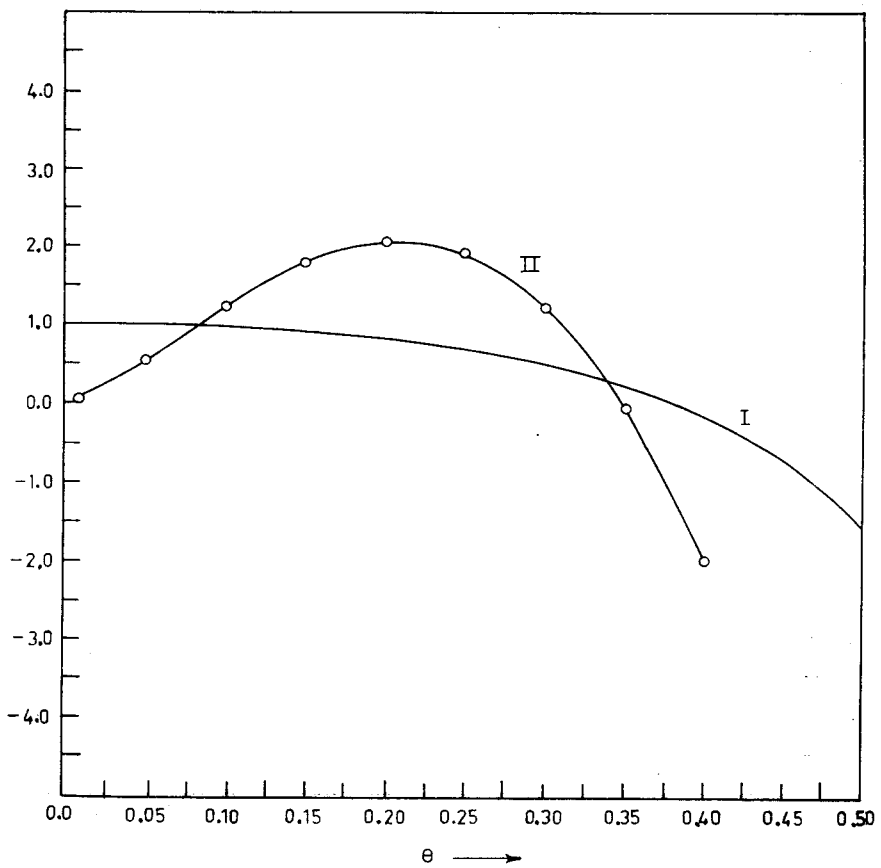

Fig. 6.2(c). The functions $Z_1(\theta)$(I) and $Z_2(\theta)$(II) against (θ) for I^-

TABLE 3. Surface coverage at which capacitance of hump occurs

Ions	Conc, N	θ_{hump} (Expt)	θ_{hump} (Present theory)
Cl^-	0.3	0.07	0.070
Br^-	0.1	0.10	0.075
I^-	0.1	0.12	0.082
ClO_3^-	0.1	0.07	0.100
BrO_3^-	0.1	0.12	0.100
NO_3^-	0.1	0.10	0.100
ClO_4^-	0.3	0.11	0.095
SCN^-	1	0.07	0.065
CN^-	0.3	0.09	0.080

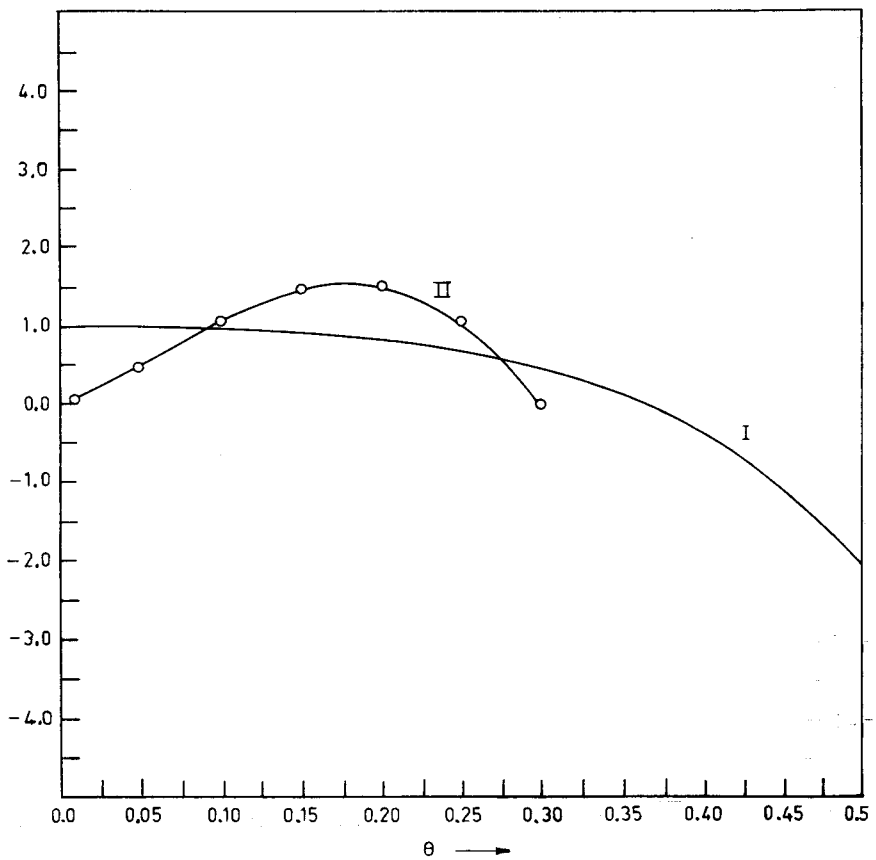

Fig. 6.2(d). The function $Z_1(\theta)$(I) and $Z_2(\theta)$(II) against σ) for ClO_3^- and BrO_3^-

where the reduced mass $M=m/2$ for an electron of mass m. The polarisability α has been taken to be non-isotropic, because of the displacement, l, in the position of the centre of the ion, due to the effect of the image field, X_{image} (cf. Fig. 6.1). The polarizability can be written as $\alpha=hr_i^3$ where the co-efficient 'h' is calculated from a knowledge of 'l' given by[1)]

$$2l^3+7r_i^2l-7r_il^2-r_i^3=0 \tag{6.4}$$

From Fig. 6.1, $\alpha=a^3=1.589r_i^3$.
Thus, knowing α, which determines D in (6.2), the roots can be found by plotting the functions

$$Z_1(\theta)=\frac{1-2\theta-\theta^2(p-1)}{(1-\theta)^2} \tag{6.5}$$

and

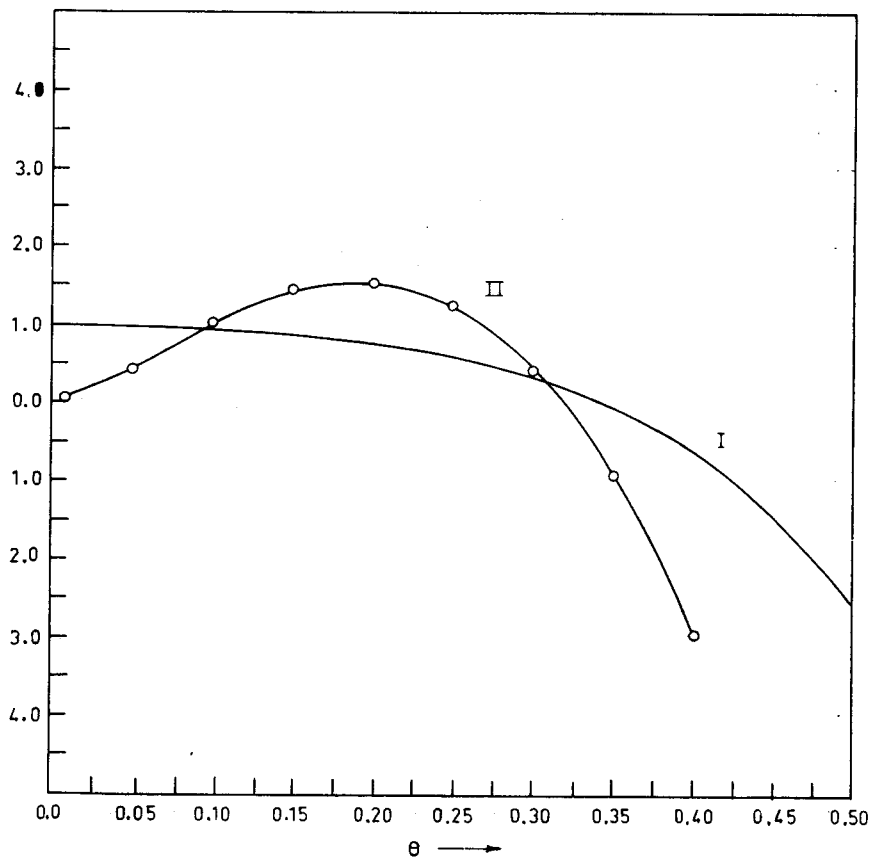

Fig. 6.2 (e). The functions $Z_1(\theta)$(I) and $Z_2(\theta)$(II) against (θ) for NO_3^-

$$Z_2(\theta)=\frac{C\sqrt{\theta}}{4}\sum_{n=1}^{\infty}\left\{\frac{1+\frac{\pi\theta}{n^2}}{\left(1+\frac{\pi\theta}{4n^2}\right)^{5/2}}-1\right\}-6D\theta^3\sum_{n=1}^{\infty}\frac{1}{n^5}\left[1+\frac{1-\frac{\pi\theta}{4n^2}}{\left(1+\frac{\pi\theta}{4n^2}\right)^{5}}\right] \tag{6.6}$$

against θ.

In Fig. 6.2 (a–g), $Z_1(\theta)$ and $Z_2(\theta)$ are plotted against θ for various anions; the radii and other calculated parameters are given in Table 1. For all the ions examined, the functions $Z_1(\theta)$ and $Z_2(\theta)$ intersects at two points, i. e., we get two roots θ_1 and θ_2 of eqn. 6.2 and thus *two* inflection points on the θ–q_M curve. The values of θ_1 and θ_2 for the anions are given in Table 2 and 4 respectively.

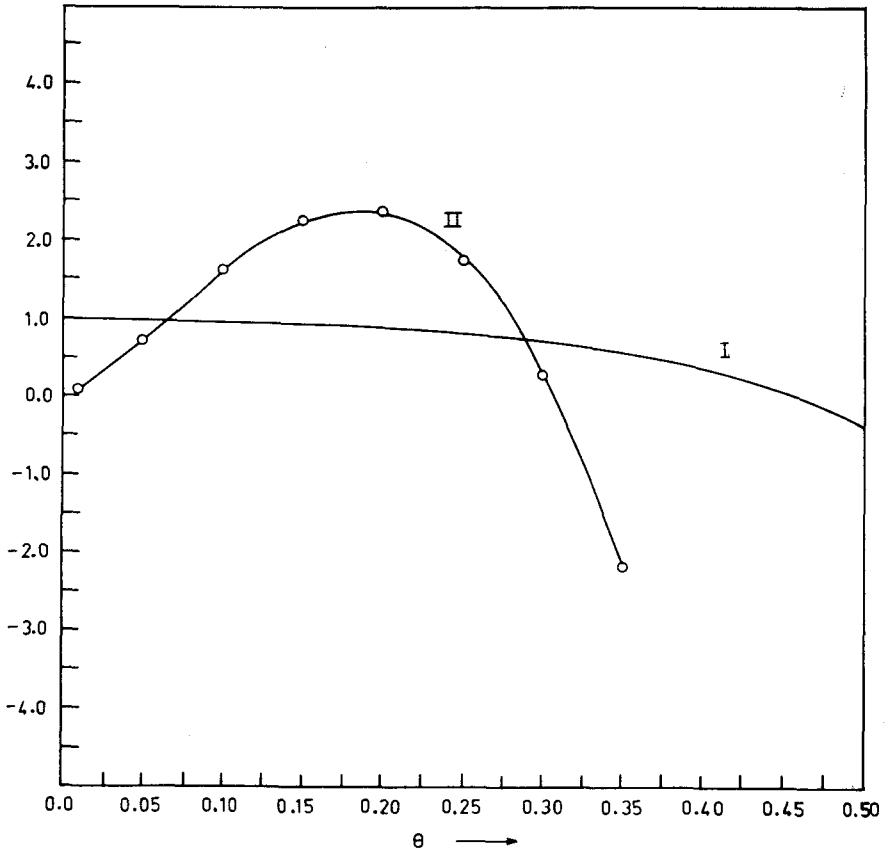

Fig. 6.2 (f). The functions $Z_1(\theta)$(I) and $Z_2(\theta)$(II) against (θ) for SCN^-

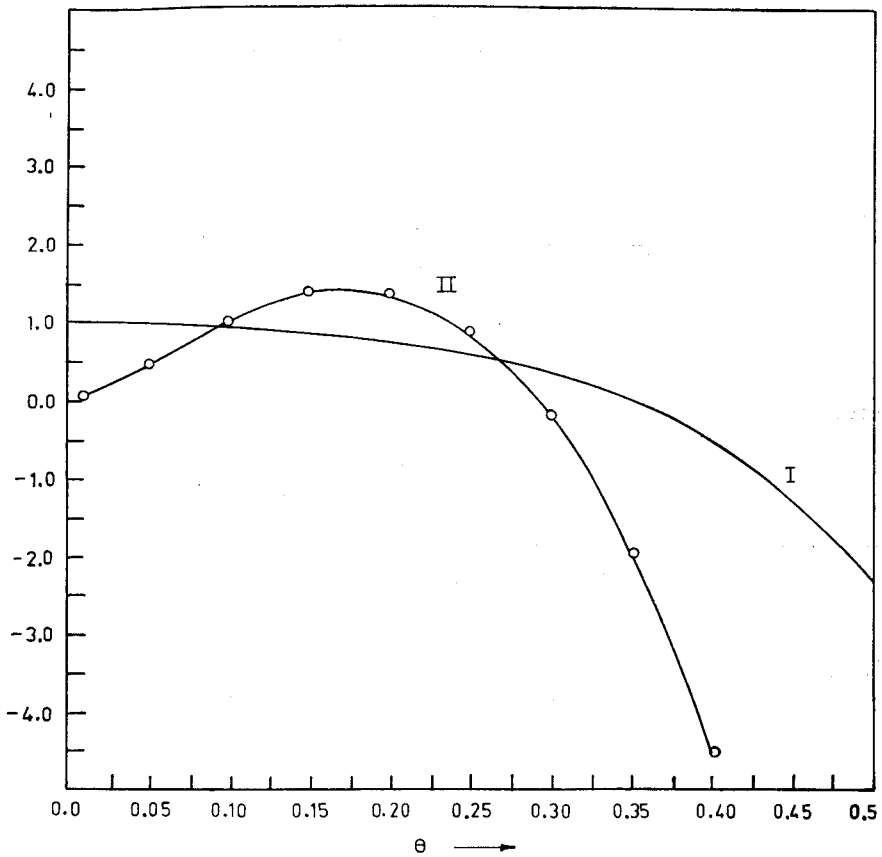

Fig. 6.2(g). The functions $Z_1(\theta)$(I) and $Z_2(\theta)$(II) against (θ) for ClO_4^-

7. Significance of θ_1

The double layer capacitance as a function of electrode charge can be represented (Appendix I) as:

$$\frac{1}{C_{DL}} = \frac{1}{K_{M\text{-}OHP}} + \frac{1}{K_{IHP\text{-}OHP}} \frac{dq_{CA}}{dq_M} + q_M \cdot \frac{d}{dq_M}\left(\frac{1}{K_{M\text{-}IHP}}\right) \qquad (7.1)$$

where $K_{M\text{-}OHP}$ and $K_{IHP\text{-}OHP}$ are integral values of the indicated capacities in the double layer.

One may show numerically[29] that the variation of the first and third terms in eqn. (7.1) are negligible compared with that of the second term. Therefore, the maxima and minima of C_{DL} depend only on $d|q_{CA}|/dq_M$ given by $d^2\theta/dq_M^2=0$. The two roots obtained numerically from eqn. (6.2)

therefore correspond to the maxima and minima on the C_{DL} versus q_M curve. To distinguish between the character of the inflections, we evaluate $d^3\theta/dq_3^M$. We rewrite the eqn. (6.1) as

$$\frac{d\theta}{dq_M} = \frac{A}{y} \tag{7.2}$$

where

$$y = \frac{1+\theta(p-1)}{\theta(1-\theta)} + \frac{C}{2\sqrt{\theta}} \sum_{n=1}^{\infty} \left\{1-\left(1+\frac{\pi\theta}{4n^2}\right)^{-3/2}\right.$$
$$\left. -3D\theta^2 \sum_{n=1}^{\infty} \frac{1}{n^5}\left\{1+\left(1+\frac{\pi\theta}{4n^2}\right)^{-4}\right\}\right. \tag{7.3}$$

Therefore,

$$\frac{d^2\theta}{dq_M^2} = -\frac{A}{y^2}\frac{dy}{dq_M} = -\frac{A}{y^2}\frac{dy}{d\theta}\cdot\frac{d\theta}{dq_M} = -\frac{A^2}{y^3}\frac{dy}{d\theta} \tag{7.4}$$

Differentiating (7.4) once more, we get

$$\frac{d^3\theta}{dq_M^3} = \frac{d}{dq_M}\left[\frac{d^2\theta}{dq_M^2}\right] = \frac{3y}{A}\left[\frac{d^2\theta}{dq_M^2}\right]^2 - \frac{A^3}{y^4}\cdot\frac{d^2y}{d\theta^2} \tag{7.5}$$

$d^2\theta/dq_M^2$ at the inflection point is zero, therefore, the sign of the values of the term $-(A^3/y^4)(d^2y/d\theta^2)$ will determine the maximum and minimum. But A^3/y^4 being always positive, the sign of $-d^2y/d\theta^2$ for θ_1 and θ_2 is the determining factor for the maximum or minimum on the capacitance charge curve.

Double differentiation of eqn. (7.3) w. r. t. θ and multiplication by -1 gives rise to

$$-\frac{d^2y}{d\theta^2} = \frac{6\theta-6\theta^2-2\theta^3(p-1)-2}{\theta^3(1-\theta)^3} - \frac{3}{8}\frac{C}{\theta^{5/2}}\sum_{n=1}^{\infty}\left[1-\frac{\frac{\pi\theta}{n^2}\left\{1+\frac{\pi\theta}{2n^2}\right\}+1}{\left[1+\frac{\pi\theta}{4n^2}\right]^{7/2}}\right]$$
$$+6D\sum_{n=1}^{\infty}\frac{1}{n^5}\left[1+\frac{1}{\left[1+\frac{\pi\theta}{4n^2}\right]^6}\left\{1-\frac{3}{2}\frac{\pi\theta}{n^2}+\frac{3\pi^2\theta^2}{(4n^2)^2}\right\}\right] \tag{7.6}$$

The values of $-d^2y/d\theta^2$ calculatded from eqn. (7.6) for θ_1 are given in table 2. θ_1 for all the investigated anions gives a negative value of $-d^2y/d\theta^2$. Therefore, the root θ_1 corresponds to maximum (or hump) on the capacitance charge curve.

In Table 3, the results of the present model have been compared with experiment. Agreement is good.

8. Significance of θ_2

Substituting the values of θ_2 in eqn. (7.6), we have calculated the value of $-d^2y/d\theta^2$. It is positive for all ions (Table 4), i. e., θ_2 represents a minimum in the eqn. 6.1 and, therefore, from 7.1, of C_{DL} in the C_{DL}–q_M curve.

To examine the degree of consistency between the calculated values of θ_2, and the observed capacitance minimum, the observed q_M's at which C_{DL} passes through a minimum were found. From experimental $q_{CA}-q_M$ plots and equation

TABLE 4. The values of $-d^2y/d\theta^2$ and constituent terms in eqn. (7.6) corresponding to θ_2

Ions	θ_2	1st term	2nd term	3rd term	$-d^2y/d\theta^2$
Cl^-	0.3100	−77.6059	−218.1215	151.6871	292.2027
Br^-	0.3200	−73.7565	−191.4286	133.5688	251.2408
I^-	0.3350	−70.3362	−158.9041	112.1764	200.7443
ClO_3^- & BrO_3^-	0.2700	−117.5481	−202.1399	138.2546	222.8464
ClO_4^-	0.2750	−113.9599	−188.0315	137.1058	211.1774
NO_3^-	0.3050	−91.8189	−155.3257	112.1067	175.6135
SCN^-	0.2850	−93.7283	−282.1875	197.6039	386.0631

TABLE 5*. Positions of the capacitance minimum

	Ions	q_M at C_{min} Expt in $\mu c/cm^2$	q_{CA} at C_{min} Expt ($\mu c/cm^2$)	θ_2 Expt	θ_2 Calc	Ref. for q_M	Ref. for q_{CA}
Monoatomic Ions	Cl^-	10.0	12.4	0.100	0.310	11, 30	27, 34, 36
	Br^-	7.0	14.0	0.135	0.320	34, 35	
	I^-	3.0	16.0	0.192	0.335	30	
Polyatomic Ions	ClO_3^-	13.0	8.0	0.110	0.270	36	27
	BrO_3^-	11.6	9.5	0.145	0.270	36	27
	ClO_4^-	11.5	15.0	0.240	0.275	37	27
	NO_3^-	11.1	15.0	0.256	0.305	28	39
	SCN^-	20.0	31.0	0.198	0.285	38	27

* The expt. values are for solution of 0.1N concentration. θ_{min} increases with increase of ionic radii with the exception of SCN^-. Probably the linear SCN^- ion does not adsorb normal to the surface but adsorb flat to the surface so that the effective radii is higher than 1.6 Å.

$$-q_{CA} = \theta N_T e = \frac{e}{4r_i^2}\theta \qquad (8.1)$$

one can find the experimental θ_{min} (Table 5). Thus, although θ_2 is higher than $\theta_{min,expt}$, with increase of r_i, $\theta_{min,expt}$ and θ_2 both increase. The discrepancy may arise from the rudimentary calculation of the ion-ion dispersive energy which only takes into account the outershell electrons.

9. Dependence of Hump and Minimum on Temperature

The capacitance hump and consequently the capacitance minimum disappear with increase of temperature.[28] Due to the availability of experimental data, the NO_3^- ion is taken up for theoretical investigation of the

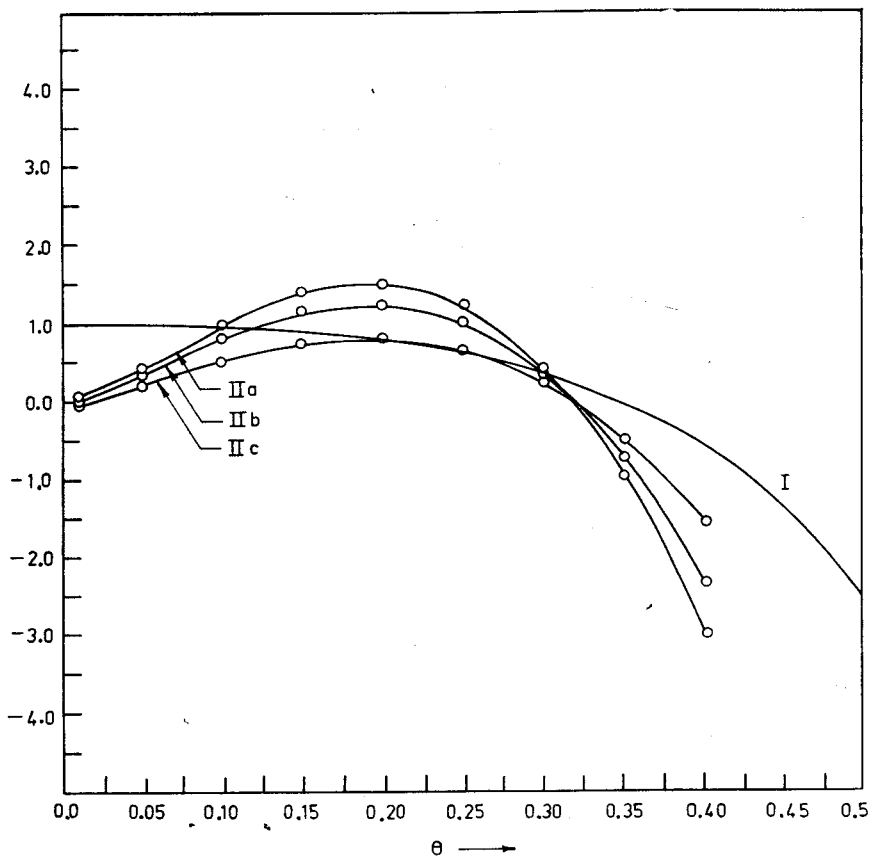

Fig. 9.1. Plots of $Z_2(\theta)$ at temperatures 25°C (II a), 100°C (II b) and 300°C (II c) and $Z_1(\theta)$(I) against θ.

effect of temperature on capacitance hump and minimum. In Fig. 9.1, θ_1 and θ_2 are shown at different temperatures. With increase of temperature θ_1 and θ_2, i. e., hump and minimum, come closer to each other and disappear, as found experimentally.[28]

10. A Comparison of Models

The approach used by LEVINE *et al.*[5] takes into account all possible interactions including lateral repulsion. Several approximations chosen in the calculation may be questioned. For example, LEVINE assumed $r_0=\infty$, which is tantamount to assuming $\kappa=0$ in the electrolyte theory. The question of graininess at the actual distances apart of the ions concerned is not considered. The model tends to over-estimate the imaging energy in solution, as first stated by MACDONALD and BARLOW,[3,4] (See Section 2.).

The alternative approximation of BOCKRIS, DEVANATHAN and MULLER[1] neglects the imaging in solution, because it was pre-supposed that the absence of any sharp boundary would greatly reduce imaging in the solution, and therefore multiple imaging (section 2). In the BDM[1] approach, therefore, only the interaction of adsorbed ion with the surrounding counter adsorbed ions, and with their images in metal are considered (together with the electrical work of transfer of ion from the solution to the electrode). In the present version of this approach the coulombic repulsion of the ions is worked out without approximations in single imaging; and the ion-ion dispersive interaction is included to interpret the capacitance minimum. The BDM approach underestimates the imaging energy by about 1%, and LEVINE *et al.* overestimate it by about 40%.

Recenlty, LEVINE[6] and co-workers[40,44] have attempted to overcome the difficulties arising from their original model and the sharp boundary. They have recently assumed an arbitrary variation of dielectric constant, as a function of distance from the electrode, but used fixed values of dielectric constants (termed mean values) ε_1 and ε_2 over certain arbitrary distances, implying dielectric discontinuity at an arbitrary point in the inner region and at OHP. This refers to an interface represented in figure (2.2.1). In such a case, the total multiple image interaction energy of an ion on the IHP is given by the eqn. (2.2.6). With $\varepsilon_1=6$, $\varepsilon_2=50$, $\varepsilon_3=80$ and $a=x_1=d=2$Å, we fiind from (2.2.6) $E_{12}=-(e^2/\varepsilon_1)\,(0.3275\times10^8\,\mathrm{cm})=1.31E_S$, where the single image interaction energy, E_S, is given by (2.5.11). This is to be compared with the value of $E_{11}=1.38E_S$, the interaction energy obtained with one sharp dielectric discontinuity, and with E_T (smooth dielectric variation)$=1.01E_S$. Thus, if there are *two* sharp boundaries, it is still

important to use multiple imaging, as it is for one sharp boundary. However, in the physical situation, the existence of sharp dielectric boundary is unknown, and the appropriate analysis for the imaging contribution to the double layer properties should be done using a dielectric situation described in section 2 (*continuous* variation) and, in that case, the multiple imaging contribution constitutes only a 1% addition to the single imaging. The recent approach of LEVINE *et al.* therefore still greatly overestimates the imaging energy.

In the approach used by LEVINE[42], the anodic capacitance hump was interpreted in terms of water molecule capacitance which contradicts the experimental fact[7] that the water molecules are most randomly oriented at a potential negative to the p. z. c. (maximum in solvent excess entropy passes through a maximum at $q \simeq -4\mu c/\mathrm{cm}^2$). However, it is easy to show that the LEVINE[5] isotherm does give a capacitance hump (independent of water molecules) and this provides a useful criterion of the relative validity of the sharp dielectric (LEVINE) and diffuse dielectric (BOCKRIS) models.

Thus, the LBC isotherm can be written as[2],

$$\ln \frac{\theta}{(1-p\theta)^p} = -\frac{\Delta G_c^0}{kT} + \ln \frac{a_\pm}{a_0} + A' q_M - C'\theta + \frac{e\phi_{diff}}{kT} \qquad (10.1)$$

where $A' = 4\pi e\gamma/\varepsilon kT$, $\gamma \equiv d - r_i$ where d is the distance between the electrode and OHP, $C' = 4\pi\gamma e q_{max}\,(1 - r_i/d)/\varepsilon kT$ and ϕ_{diff} is the mean potential at the OHP, and ΔG_c^0 has the same significance as in eqn. (5.13).

(i) *Prediction of inflection points on the θ vs q_M curve*

With $p=2$, as suggested by LEVINE[6], and neglecting ϕ_{diff} for a fairly concentrated solution, the isotherm (10.1) takes the form

$$\ln \frac{\theta}{(1-2\theta)^2} = \text{constant} + \ln\, a_\pm + A' q_M - C'\theta \qquad (10.2)$$

Differentiation of (10.2) w. r. t. q_M gives

$$\frac{d\theta}{dq_M} = \frac{A'}{\frac{1}{\theta} + \frac{4}{1-2\theta} + C'} \qquad (10.3)$$

Therefore,

$$\frac{d^2\theta}{dq_M^2} = \frac{-A'^2(4\theta^2 + 4\theta - 1)}{\left(\frac{1}{\theta} + \frac{4}{1-2\theta} + C'\right)^3 \theta^2 (1-2\theta)^2} \qquad (10.4)$$

Using the condition, $d^2\theta/dq_M^2 = 0$, an inflection on θ–q_M curve can occur only when

$$4\theta^2+4\theta-1=0 \tag{10.5}$$

The eqn. (10.5) has got two roots*),

$$\theta_1=\frac{1}{2}(\sqrt{2}-1)=0.207 \text{ and } \theta_2=-\frac{1}{2}(\sqrt{2}+1)=-1.207 \tag{10.6}$$

A negative value of θ has no physical significance. Using eqn. (10.5) $q_{CA,in\,fl}$ does not depend on the nature of the anion which is contrary to experiment.[27]

(ii) *Predicition of the hump and the minimum on* C_{DL}–q_M *curve*

To find whether the inflection point predicted by equation (10.2) corresponds to a maximum or minimum on the C_{DL}–q_M curve we differentiate (10.4) to get

$$\frac{d^3\theta}{dq_M^3}=+\frac{3A'}{y'}\cdot\left(\frac{d^2\theta}{dq_M^2}\right)^2-\frac{A'^3}{y'^4}\cdot\frac{d^2y}{d\theta^2} \tag{10.7}$$

where

$$y'=\frac{1}{\theta}+\frac{4}{1-2\theta}+C' \tag{10.8}$$

For either maximum or minimum, $d^2\theta/dq_M^2=0$ and hence the sign of the quantity $-(A'^3/y'^4)(d^2y'/d\theta^2)$ determines whether the root represents delete maxima or minima. A'^3/y'^4 being always positive, the maxima or minima is determined by the sign of $-d^2y'/d\theta^2$. Double differentiation of (10.8) and multiplication by -1 gives

$$-\frac{d^2y'}{d\theta^2}=-\left[\frac{2}{\theta^3}+\frac{32}{(1-2\theta)^3}\right] \tag{10.9}$$

Substituting the value of θ_1 in (10.9), numerical calculution shows that (10.9) is always negative, and hence the root θ_1 corresponds to a maximum on the C_{DL}–q_M curve. Moreover θ_1 being independent of the nature of the anion, the capacitance maximum predicted by eqn. (10.2) is independent of the anion, and thus is contrary to experiment. θ_1 is also numerically too high (Table 3). No capacitance minimum is predicted. Disappearance of capacitance hump and minimum with rise of temperature also cannot be rationalized from (10.2).

It is, therefore, delete clear that the isotherm deduced on the basis of the sharp dielectric boundary is able to rationalize to capacitance-charge dependence less well than that based on the diffuse dielectric boundary which corresponds delete more nearly to the real situation.

*) These properties of the equations of LEVINE *et al.* were first pointed out by R. SEN.[29]

Acknowledgement

Thanks are due to Professor H. BLEVIN for suggesting the method for image calculation and to Dr. K. GOPALSAMY for mathematical discussions. One of us (M. A. H.) is grateful to Flinders University for a research scholarship.

Appendix I

The Effect of Integral Capacitance on the Capacitance-Charge Relation

For a concentrated solution, the diffuse layer p. d. being very small, one can represent the p. d. across the electrode solution interface as[30]

$$\phi_M-\phi_S=\frac{4\pi x_1 q_M}{\varepsilon_1}+\frac{4\pi(x_2-x_1)(q_M+q_{CA})}{\varepsilon_2} \qquad (i)$$

where ε_1 and ε_2 are the dielectric constants in the region between the metal and the IHP and that between IHP and OHP respectively.

Using $1/K_{M\text{-}IHP}=4\pi x_1/\varepsilon_1$ and $1/K_{IHP\text{-}OHP}=4\pi(x_2-x_1)/\varepsilon_2$, the eqn. (i) can be rewritten as

$$\phi_M-\phi_S=\frac{q_M}{K_{M\text{-}IHP}}+\frac{q_M+q_{CA}}{K_{HIP\text{-}OHP}}=q_M\left[\frac{1}{K_{M\text{-}IHP}}+\frac{1}{K_{IHP\text{-}OHP}}\right]+\frac{q_{CA}}{K_{IHP\text{-}OHP}} \qquad (ii)$$

Differentiating w. r. t. q_M, we find

$$\frac{d(\phi_M-\phi_S)}{dq_M}=\frac{1}{C_{DL}}=\frac{1}{K_{M\text{-}IHP}}+q_M\cdot\frac{d}{dq_M}\left[\frac{1}{K_{M\text{-}IHP}}\right]+\frac{1}{K_{IHP\text{-}OHP}}\left[1+\frac{dq_{CA}}{dq_M}\right]+[q_M+q_{CA}]\frac{d}{dq_M}\left[\frac{1}{K_{IHP\text{-}OHP}}\right] \qquad (iii)$$

The plot of $\phi_M-\phi_S$ against q_{CA} yields straight lines[31,43] having equal slopes which is the value of $1/K_{IHP\text{-}OHP}$ for various values of q_M. Thus $1/K_{IHP\text{-}OHP}$ may be considered as independent of q_M; hence

$$\frac{d[1/K_{IHP\text{-}OHP}]}{dq_M}=0 \qquad (iv)$$

Then with the identity

$$\frac{1}{K_{M\text{-}OHP}}=\frac{1}{K_{M\text{-}IHP}}+\frac{1}{K_{IHP\text{-}OHP}}\text{*)} \qquad (v)$$

*) From eqn. (iv) and (v), one can also have

$$\frac{d}{dq_M}\left[\frac{1}{K_{M\text{-}OHP}}\right]=\frac{d}{dq_M}\left[\frac{1}{K_{M\text{-}IHP}}\right] \qquad (va)$$

one can write (iii) as

$$\frac{1}{C_{DL}} = \frac{1}{K_{M\text{-}OHP}} + \frac{1}{K_{IHP\text{-}OHP}} \frac{dq_{CA}}{dq_M} + q_M \cdot \frac{d}{dq_M}\left[\frac{1}{K_{M\text{-}IHP}}\right] \qquad \text{(vi)}$$

Assuming the identity (va), SEN[29] evaluated the contribution of $q_M d(1/K_{M\text{-}OHP})/dq_M$ to the capacity by using the variation of $K_{M\text{-}OHP}$ with q_M for Cl^- ion given by GRAHAME and PARSONS[31] and showed that the term does give a hump, but its magnitude is very small compared with the observed one. The type of data obtained for other ions[32] is of similar magnitude to that for Cl^-. Since $d(1/K_{M\text{-}OHP})/dq_M$ i. e., the slope of $1/K_{M\text{-}OHP}$ versus q_M plot is very small in comparison with the term dq_{CA}/dq_M, the slope of $q_M - q_{CA}$ plot, which has the values 1 to 2 in the anodic region, one can conclude that dq_{CA}/dq_M is the major term controlling the variation of C_{DL} with q_M on the anodic side of p. z. c.

References

1) J. O'M. BOCKRIS, M. A. V. DEVANATHAN and K. MULLER, Prc. Roy. Soc., A **274**, 55 (1963).
2) H. WROBLOWA, and K. MULLER, J. Phys. Chem., **73**, 3528 (1969).
3) C. A. BARLOW, J. R. MACDONALD, J. Chem. Phys., **40**, 1535 (1964).
4) C. A. BARLOW and J. R. MACDONALD, J. Chem. Phys., **43**, 2575 (1965).
5) S. LEVINE, G. M. BELL and D. CALVERT, J. Chem., **40**, 518 (1962).
6) S. LEVINE, J. Colloid and Interface Sci., **37**, 619 (1971).
7) R. M. REEVES, Modern Aspects of Electrochem., Vol. 9, Edt. J. O'M. BOCKRIS and B. E. CONWAY, Plenum Press, N. Y. (1974).
8) D. J. SCHIFFRIN, Trans. Farad. Soc., **67**, 3318 (1971).
9) J. A. HARRISON, J. E. B. RANDLES and D. J. SCHIFFRIN, J. Electroanal. Chem., **48**, 359 (1973).
10) G. J. HILLS, J. Phys. Chem., **73**, 3591 (1969).
11) G. I. HILLS and R. PAYNE, Trans. Farad. Soc., **61**, 326 (1965).
12) J. O'M. BOCKRIS and M. A. HABIB, J. Electroanal. Chem. and Interfacial Electrochem. to be published (1975).
13) P. J. FLORY, J. Chem. Phys., **10**, 51 (1942); M. L. HUGGINS, N. A. Ann, Acad. Sci., **43**, 1 (1942).
14) E. BLOMGREN and J. O'M. BOCKRIS, J. Phys. Chem., **63**, 1475 (1959).
15) G. GOUY, J. Chim. Phys. (Paris), **29** (7), 145 (1903); D. L. CHAPMAN Phil. Mag.**25** (6), 475 (1913).
16) F. BOOTH, J. Chem. Phys., **19**, 391, 1327, 1615 (1951).
17) D. C. GRAHAME, J. Chem. Phys., **18**, 903 (1950).
18) T. LAIDLER, Can. J. Chem., **37**, 138 (1959).
19) W. R. SMYTHE, Static and dynamic electricity, 3rd Edn. McGraw Hill Book Co. (1968).

20) S. LEVINE, K. ROBINSON, Electroanal. Chem., **41**, 159 (1973).
21) F. P. BUFF and F. H. STILLINGER, J. Chem. Phys., **39**, 1911 (1963).
22) J. O'M. BOCKRIS and A. K. N., REDDY, Modern Electrochem. Plenum/Roseta Edn., Plenum Press, N. Y. (1973).
23) J. C. SLATER and J. G. KIRKWOOD, Phys. Rev., **37**, 682 (1931).
24) R. A. PIEROTTI and G. D. HALSEY, Jr., J. Phys. Chem., **63**, 680 (1959).
25) D. EISENBERG and W. KAUZMAN, The Structure and Prop. of Water, Oxford Univ. Press, 1969.
26) H. P. DHAR, B. E. CONWAY and K. M. JOSHI, Electrochem. Acta, **18**, 789 (1973).
27) H. WROBLOWA, Z. KOVAC and J. O'M. BOCKRIS, Trans. Farad. Soc., **61**, 1523 (1965).
28) D. C. GRAHAME, J. Am. Chem. Soc., **79**, 2093 (1957).
29) R. K. SEN, Dissertation, Univ. Pennsylvania 1972.
30) M. A. V. DEVANATHAN, Trans. Farad. Soc., **50**, 373 (1954).
31) D. C. GRAHAME and R. PARSONS, J. Am. Chem. Soc., **83**, 1291 (1961).
32) Z. KOVAC, Ph. D. Dissertation, pp. 230, Univ. of Pennsylvania, 1964.
33) R. PAYNE, J. Phys. Chem., **69**, 4113 (1965).
34) J. LAWRANCE, R. PARSON, and R. PAYNE, J. Electroanal. Chem., **16**, 193 (1968).
35) A. R. SEARS and P. A. LYONS, J. Electroanal. Chem., **42**, 69 (1973).
36) A. WATANABE, F. TSUJI and U. SHIZUO, Proceedings of the Second International Congress of Surface Activity, Vol. III, 94 (1957), Butterworths & Co. (London).
37) D. C. GRAHAME, Chem. Rev., **41**, 441 (1947).
38) R. PARSONS and P. C. SYMONS, Trans. Farad. Soc., **64**, 1077 (1968).
39) R. PAYNE, J. Electrochem. Soc., **118**, 999 (1966).
40) K. ROBINSON and S. LEVINE, Electroanal. Chem. and Interfacial Electrochem., **47**, 395 (1973).
41) B. E. CONWAY, J. O'M. BOCKRIS and I. A. AMMAR, Trans. Farad. Soc., **47**, 756 (1951).
42) S. LEVINE, G. M. BELL and A. L. SMITH, J. Phys. Chem., **73** 3534 (1969).
43) D. C. GRAHAME, J. Am. Chem. Soc., **80**, 4201 (1958).
44) S. LEVINE and K. ROBINSON, J. Electroanal. Chem., **54**, 237 (1974).